

**Excitonic stimulated emission from  $\text{Mg}_x\text{Zn}_{1-x}\text{O}$  films due to enhanced exciton binding energy**Shusuke Fujii,<sup>1</sup> Yutaka Adachi,<sup>2</sup> and Takashi Uchino<sup>1,\*</sup><sup>1</sup>*Department of Chemistry, Graduate School of Science, Kobe University, Nada, Kobe 657-8501, Japan*<sup>2</sup>*Optoelectronic Materials Group, Optical and Electronic Materials Unit, National Institute for Materials Science, Tsukuba, Ibaraki 305-0044, Japan*

(Received 9 April 2020; revised 21 July 2020; accepted 21 July 2020; published 6 August 2020)

We report synthesis and excitonic emission properties of high-quality micrometer-thick  $\text{Mg}_x\text{Zn}_{1-x}\text{O}$  films ( $x = 0.04$  and  $0.10$ ) grown on *a*-sapphire substrates by pulsed laser deposition. The band gap  $E_g$  values of the  $x = 0.04$  and  $0.10$  samples have been shown to be larger than that of pure ZnO by  $\sim 0.1$  and  $\sim 0.3$  eV, respectively. From the investigations of the stimulated emission due to the exciton-exciton (ex-ex) scattering process at 3 K, the exciton binding energies  $E_b$  of the  $x = 0.04$  and  $0.10$  samples are determined to be  $80 \pm 5$  and  $120 \pm 10$  meV, respectively, which are substantially larger than that of pure ZnO ( $E_b = 60$  meV). The present observation demonstrates that  $E_b$  of ZnO-based materials can be increased to 100% by controlling the synthetic and alloying conditions. Purely excitonic stimulated emissions are observed in the temperature range from 3 to 300 K without showing any symptoms of electron-hole plasma emission. The mechanism of the optical gain changes from the ex-ex to ex-electron (ex-el) scattering process at 200 and 250 K for the  $x = 0.04$  and  $0.10$  samples, respectively, with increasing temperature. We argue that the enhancement of  $E_b$  occurs as a consequence of a complex, combined effect of Mg addition on the effective electron/hole masses and the dielectric constant of the  $\text{Mg}_x\text{Zn}_{1-x}\text{O}$  films.

DOI: [10.1103/PhysRevB.102.075204](https://doi.org/10.1103/PhysRevB.102.075204)**I. INTRODUCTION**

Dynamics and properties of excitons and their related optical processes in semiconductors in various forms, such as bulk, thin films, and nanostructures, have been the subject of investigations in terms both of fundamental physics [1–4] and of practical optoelectronic applications [5]. Among other semiconductors, ZnO has attracted considerable interest because of its large exciton binding energy  $E_b$  of 60 meV [6–8], which can offer the possibility of efficient excitonic lasing operating at room temperature [9,10]. As for room-temperature stimulated emission from ZnO, however, there has been controversy about the role of excitons in optical gain [9–13]. Klingshirn and coworkers [12,13] have proposed that at 300 K the exciton binding energy vanishes when the electron-hole pair density  $n_p$  approaches  $n_p \sim 10^{17} \text{ cm}^{-3}$ , which is a typical density at which stimulated emission is claimed to occur in ZnO at room temperature. The value of  $n_p \sim 10^{17} \text{ cm}^{-3}$  is almost comparable to the Mott density  $n_M$  [14], where excitons merge into the continuum and dissociate into electron-hole plasma (EHP). Thus, the  $E_b$  value of 60 meV may not be sufficiently large to guarantee the occurrence of excitonic stimulated emission at room temperature.

Hence, it is desirable to increase the  $E_b$  value more than 60 meV to unambiguously realize the room-temperature excitonic stimulated emission. Also, a large exciton binding energy is preferable to operate any exciton-related devices at room temperature. One promising method for enhancing

$E_b$  is to utilize the quantum-confinement effect in multiple-quantum well (MQW) structures [15]. Sun *et al.* [16] have shown that the  $E_b$  value can be raised to 86 meV in well-designed ZnO/MgZnO MQWs. Even in the case of the MQWs, however, purely excitonic stimulated emissions were realized only at temperatures below  $\sim 160$  K; at temperatures above  $\sim 200$  K, both the excitonic and inverted EHP emissions were found to contribute to the optical gain [16]. The other method for enhancing  $E_b$  is band-gap widening by alloying with an oxide with a wider band gap, such as MgO or BeO since, in general,  $E_b$  increases with increasing band-gap energy  $E_g$  [17,18]. Such band-gap engineered materials are also interesting in terms of tuning of the excitonic emission energy. It has been reported that the  $E_b$  value of MgZnO alloys becomes larger than that of pure ZnO [19,20], although there exists a report that  $E_b$  shows a negative bowing effect for increasing Mg mole fraction [21]. Previously, the emission properties of  $\text{Mg}_x\text{Zn}_{1-x}\text{O}$  thin films with thickness of 500–600 nm have been investigated [22,23]. In these studies [22,23], stimulated emission was found to occur at room temperature; however, a broad and redshifted emission band, which is characteristic to an inverted EHP emission, was also developed with increasing excitation intensity above threshold. This implies that in these thin-film samples a possible effect of an increase in  $E_b$  is overwhelmed by alloying effects, i.e., deterioration of crystallinity and optical quality due to solute atoms.

In this work, we investigate the stimulated emission characteristics of  $\text{Mg}_x\text{Zn}_{1-x}\text{O}$  thin films with thickness over  $\sim 1 \mu\text{m}$ . These micrometer-thick films have an advantage over the often-studied hundreds-of-nanometer-thick films [22,23] in terms of excitonic stimulated emission because of the inher-

\*uchino@kobe-u.ac.jp

ent high crystalline quality and low-loss feedback mechanism, as has been proved by the present authors using  $\mu\text{m}$ -sized ZnO particles and films [24,25]. We demonstrate that the  $E_b$  value of the  $\text{Mg}_x\text{Zn}_{1-x}\text{O}$  films can be raised to  $\sim 120$  meV by controlling the synthetic and alloying conditions. We then analyze how the change in  $E_b$  affects the temperature dependence of the excitonic emission properties. Attention is given also to the anomalous  $E_g - E_b$  relationship observed for the present  $\text{Mg}_x\text{Zn}_{1-x}\text{O}$  films.

## II. EXPERIMENTAL PROCEDURES

### A. Sample preparation

The  $\text{Mg}_x\text{Zn}_{1-x}\text{O}$  thin films were grown on an  $a$ -plane sapphire substrate by pulsed laser deposition (PLD) using the fourth harmonic ( $\lambda = 266$  nm) of a Nd-doped yttrium aluminum garnet (Nd:YAG) laser with a pulse width of 5 ns, a repetition rate of 5 Hz, and an average fluence of about  $1 \text{ J/cm}^2$ . We used various ZnO-based targets with different MgO content ranging from 4 to 9.5 mol%. The  $\text{O}_2$  partial pressure in the growth chamber was kept constant at  $2 \times 10^{-3}$  Pa, and the substrate temperature was kept at  $450^\circ\text{C}$ . The concentration of Mg was estimated from the  $c$ -axis length deduced from x-ray-diffraction analysis and the peak energy of the donor-bound exciton recombination measured at 3 K [26,27]. In this work, we prepared the  $\text{Mg}_x\text{Zn}_{1-x}\text{O}$  thin films with compositions of  $x = 0.04$  and  $0.10$ . We performed the photoluminescence (PL) measurements for the  $x = 0.04$  sample with different thickness of 120, 300, and 1018 nm to investigate the possible effect of film thickness  $d$  on the excitonic emission properties. As for the  $x = 0.10$  samples, we only investigated the emission properties of  $\mu\text{m}$ -thick films ( $d = 1230$  nm).

### B. Characterization

The crystallinity of the film samples was characterized by x-ray diffraction (XRD) with a PANalytical X'pert Pro MRD equipped with a hybrid two-bounce asymmetric Ge (220) monochromator and Cu- $K_\alpha$  source. The optical absorption of the  $\text{Mg}_x\text{Zn}_{1-x}\text{O}$  films was measured using a monochromated Xe lamp and a lock-in amplifier with optical chopper. The temperature of the sample loaded in a He-flow cryostat was controlled with a temperature controller (Lakeshore 330) in the temperature range from 5 to 300 K. Steady-state and time-resolved PL measurements were carried out with a gated image intensified charge-coupled device (Princeton Instruments, PI-MAX:1024RB) and 1800 and 300 lines/mm gratings by using the third ( $\lambda = 355$  nm) or the fourth ( $\lambda = 266$  nm) harmonic of a Q-switched Nd:YAG laser (Spectra Physics, INDI 40, pulse width  $\sim 10$  ns, repetition rate 10 Hz) as an excitation source. During the PL measurements, the laser pulse was irradiated onto the sample surface with an incident angle of  $\sim 45^\circ$  without focusing the beam (beam spot size of  $\sim 7$  mm), and the emission signal from the front surface was monitored. The sample temperature was controlled in a closed-cycle refrigerated cryostat in the temperature range from 3 to 300 K.

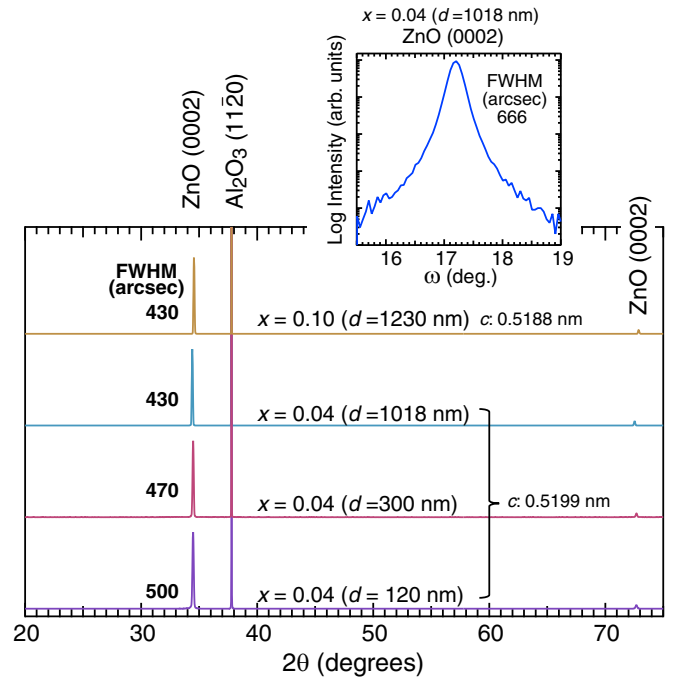


FIG. 1. XRD  $2\theta$  scans of the  $x = 0.04$  ( $d = 120$ ,  $300$ , and  $1018$  nm) and  $x = 0.10$  ( $d = 1230$  nm) samples grown on  $a$ -plane sapphire. The FWHM of the ZnO (0 0 2) reflection and the resulting  $c$ -axis length are shown. The inset shows the (0 0 2) plane rocking curve of the  $x = 0.04$  ( $d = 1018$  nm) sample.

## III. RESULTS

### A. XRD analysis

Figure 1 shows XRD  $2\theta$  scans of  $x = 0.04$  ( $d = 120$ ,  $300$ , and  $1018$  nm) and  $0.10$  ( $d = 1230$  nm) samples. Only the ZnO(0 0 0  $l$ ) reflection and the peaks from the  $a$ -plane sapphire substrate are visible in Fig. 1, indicating that all the films prepared in this work are textured with  $c$ -axis orientation perpendicular to the substrate surface. Since the position of (0 0 0  $l$ ) reflection, i.e., the  $c$ -lattice parameter, exhibits a shift from the ZnO peak position in proportion to the Mg content [26], we can evaluate the Mg content as given here. Note also that the full width at half maximum (FWHM) of the (0 0 0 2) peak shows a slight decrease from 500 to 430 arcsec as the thickness of the films increases. This implies that the structural coherence length or the grain size perpendicular to the substrate surface increases with increasing the thickness of the films. The inset in Fig. 1 shows the (0 0 0 2) plane rocking curve of the  $x = 0.04$  ( $d = 1018$  nm) sample. This rocking curve scan is sensitive to the tilt mosaic which is closely correlated to the screw dislocation density of the film. The FWHM of the XRD rocking curve  $\Delta\omega$  is 666 arcsec, which is comparable to or slightly larger than that reported previously for high-quality ZnO thin films and nanowires ( $\Delta\omega = \sim 400$ – $600$  arcsec [28,29]) This result guarantees the high crystalline quality of the present  $\mu\text{m}$ -thick  $\text{Mg}_x\text{Zn}_{1-x}\text{O}$  films.

### B. Optical absorption

Figure 2(a) shows the absorption spectra of the  $x = 0.04$  ( $d = 120$  nm) and  $0.10$  ( $d = 1230$  nm)

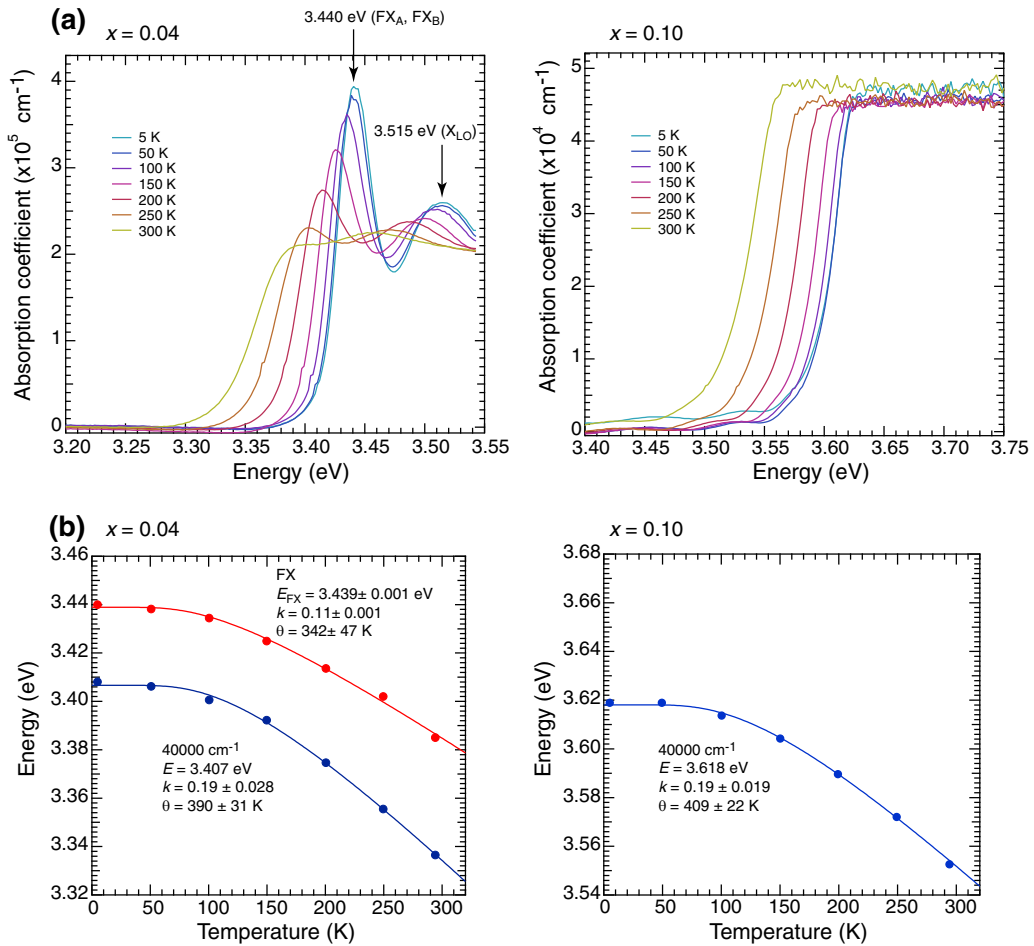


FIG. 2. (a) Absorption coefficient  $\alpha$  of the  $x = 0.04$  sample with thickness  $d = 120 \text{ nm}$  (left panel) and the  $x = 0.10$  sample with  $d = 1230 \text{ nm}$  (right panel) measured in the temperature range from 5 to 300 K. (b) Temperature dependence of the free exciton absorption peak of the  $x = 0.04$  sample (left panel). The photon energies of constant absorption  $\alpha = 40000 \text{ cm}^{-1}$  are also given as a function of temperature for the  $x = 0.04$  (left panel) and  $x = 0.10$  (right panel) samples. The solid lines and the  $E$ ,  $k$ , and  $\theta$  values indicate the results of fits of the data to Eq. (1).

samples observed in the temperature range from 5 to 300 K. In the 5-K absorption spectrum of the  $x = 0.04$  sample, one sees a strong peak at 3.440 eV, which, in analogy with the case of pure ZnO [30,31], can be attributed to the  $A$  and  $B$  free exciton absorption although the separation between these two excitons is not possible due to the limited resolution of our measurement system. Since the oscillator strength of  $C$  excitons is expected to be weak in the experimental condition used in this work (electric-field vector  $\mathbf{E} \perp c$  axis) [30], an additional higher-energy absorption at 3.515 eV will not be attributed to the  $C$  exciton; rather, it can be attributed to the longitudinal optical (LO)-phonon satellites because the energy spacing between the higher- and lower-energy peaks is  $\sim 75 \text{ meV}$ , which is in reasonable agreement with the optical-phonon energy ( $\sim 73 \text{ meV}$ ) of the  $\text{Mg}_x\text{Zn}_{1-x}\text{O}$  alloy with  $x = 0.04$  [32]. The observation of the excitonic absorptions also implies a high-quality nature of this thin-film sample. On the other hand, the 5-K absorption spectrum of the  $x = 0.10$  sample only exhibits a smooth band-edge absorption feature. This is probably because the sample is too thick ( $d = 1230 \text{ nm}$ ) to recognize strong excitonic peaks with high absorption

coefficient. Irrespective of this drawback, the effect of band-gap widening in the  $\text{Mg}_x\text{Zn}_{1-x}\text{O}$  films can be recognized in Fig. 2(a). For example, the photon energy of constant absorption  $\alpha = 40000 \text{ cm}^{-1}$  at 5 K increases from 3.408 to 3.619 eV as we go from  $x = 0.04$  to 0.10.

It is also interesting to investigate the temperature dependence of the  $A$  ( $B$ ) free exciton absorption energy ( $E_{\text{FX}}$ ) of the  $x = 0.04$  sample. Figure 2(b) demonstrates that the  $E_{\text{FX}}$  values are well fitted with the following equation given by Cody [33]:

$$E_{\text{FX}}(T) = E_{\text{FX}}(0) - \frac{k}{\exp\left(\frac{\theta}{T}\right) - 1}, \quad (1)$$

where  $\theta$  is the parameter related to the average phonon frequency and  $k$  is a dimensionless coupling constant. Equation (1) was originally proposed to predict the temperature dependence of the band gap  $E_g$  of semiconductors [33]. However, the binding energy of the free exciton  $E_b$  in ZnO is considered to be nearly independent of temperature [34]; that is, the relationship  $E_{\text{FX}}(T) = E_g(T) - E_b$  holds irrespective of temperature. Thus, Eq. (1) is often used to predict the temperature dependence of  $E_{\text{FX}}$  of pure ZnO [34]. The resulting fit-

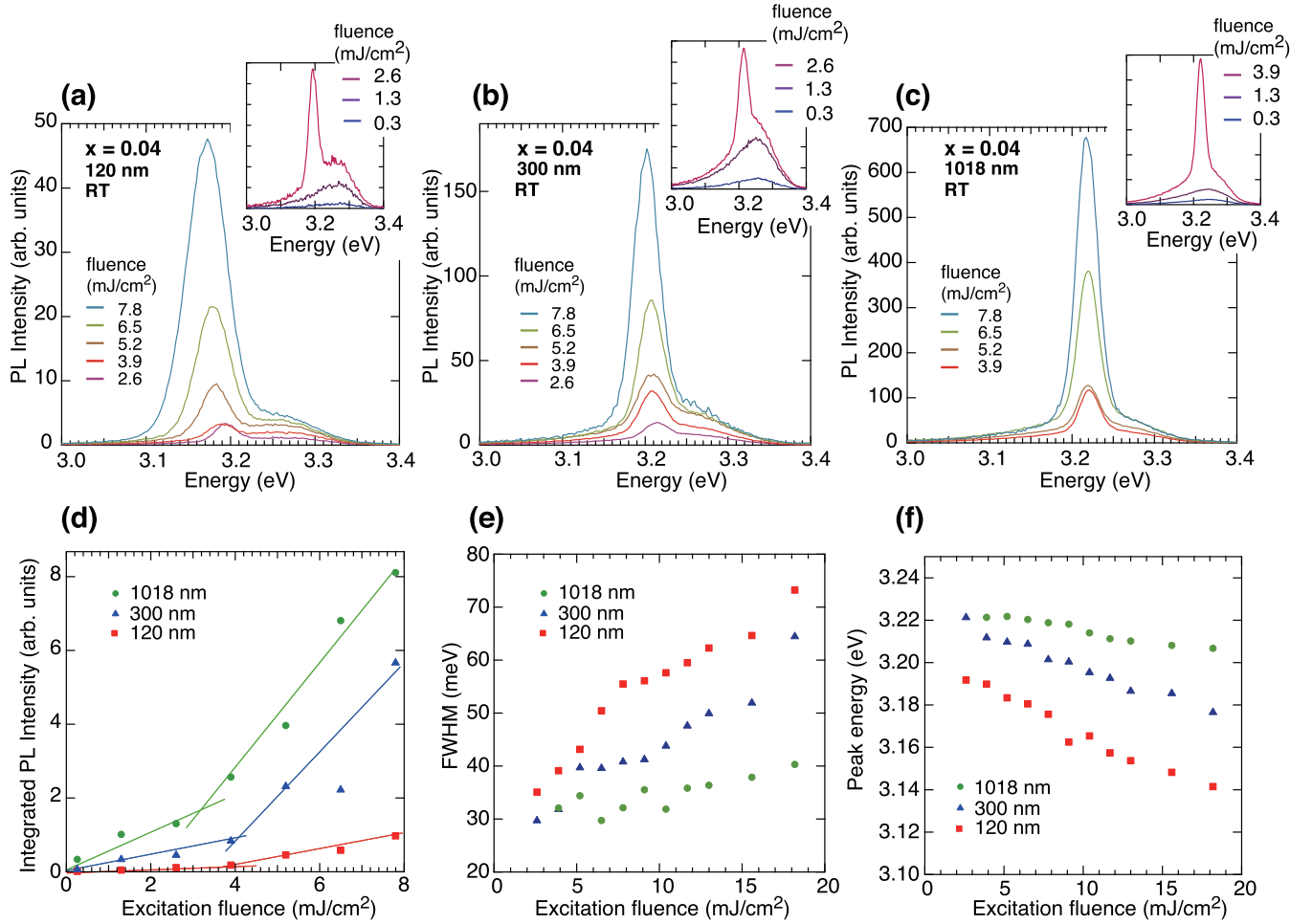


FIG. 3. Room-temperature PL spectra of the  $x = 0.04$  film samples with different thickness  $d$  under various excitation fluences; (a)  $d = 120$  nm, (b)  $d = 300$  nm, (c)  $d = 1018$  nm. The third harmonic ( $\lambda = 355$  nm) of a 10-ns pulsed Nd:YAG laser was used as an excitation source. Excitation fluence dependence of (d) the wavelength-integrated intensity, (e) the full width at half maximum (FWHM), and (f) the peak energy of the respective PL bands. In (d) and (f), the data obtained for the emission lines emerged above the threshold are shown.

ted values of  $E_{\text{FX}}(0)$ ,  $k$ , and  $\theta$  are  $0.439 \pm 0.001$  eV,  $0.11 \pm 0.001$ , and  $342 \pm 47$  K, respectively. Furthermore, we tentatively use Eq. (1) to characterize the temperature dependence of the band-tail absorption. For this purpose, we used the band-tail energy with constant absorption  $\alpha = 40\,000$   $\text{cm}^{-1}$ . The results of the curve fit are also given in Fig. 2(b). It is clear from the left panel of Fig. 2(b) that as for the  $x = 0.04$  sample, the fitted value of  $k$  for  $\alpha = 40\,000$   $\text{cm}^{-1}$  ( $k = 0.19$ ) is almost twice as large as that for  $E_{\text{FX}}$  ( $k = 0.11$ ). This indicates that the band-tail energy exhibits a stronger temperature dependence than  $E_{\text{FX}}$ . That is, excess Mg-related states along with exciton-LO phonon states are responsible for the band-tail (or Urbach tail) absorption. Figure 2(b) also reveals that the fitted values of  $k$  and  $\theta$  obtained for  $\alpha = 40\,000$   $\text{cm}^{-1}$  of the  $x = 0.04$  sample ( $k = 0.19$  and  $\theta = 390$ ) are almost identical to those of the  $x = 0.10$  sample ( $k = 0.19$  and  $\theta = 409$ ) within fitting uncertainties. Hence, it is probable that the  $x = 0.10$  sample shows a similar temperature dependence as that of the  $x = 0.04$  sample in terms not only of the band-tail absorption but also of the excitonic absorption. Hence, we assume that the fitted values of  $k$  and  $\theta$  obtained for  $E_{\text{FX}}$  of the  $x = 0.04$

sample also represent the temperature dependence of  $E_{\text{FX}}$  of the  $x = 0.10$  sample. This assumption is essential to analyze the temperature dependence of the excitonic stimulated emission of these samples, as will be shown later.

### C. Room-temperature emission characteristics

Figures 3(a)–3(c) illustrate the excitation fluence dependence of the room-temperature photoluminescence (PL) spectra of the  $x = 0.04$  samples with different values of  $d$  ( $d = 120, 300,$  and  $1018$  nm). We see from the insets of Figs. 3(a)–3(c) that under low excitation fluence  $I_{\text{exc}}$  ( $I_{\text{exc}} < \sim 1$   $\text{mJ}/\text{cm}^2$ ), all the samples show a broad PL band peaking at  $\sim 3.25$  eV irrespective of the film thickness. This broad PL band is attributed to the near-band-edge spontaneous emission due to the free exciton and its phonon replicas. When  $I_{\text{exc}}$  exceeds  $\sim 3$   $\text{mJ}/\text{cm}^2$ , a rather sharp peak appears on the lower energy side of the respective broad PL bands. As shown in Fig. 3(d), all the samples show a threshold behavior in the integrated PL intensity, implying the occurrence of stimulated emission. It should be noted,

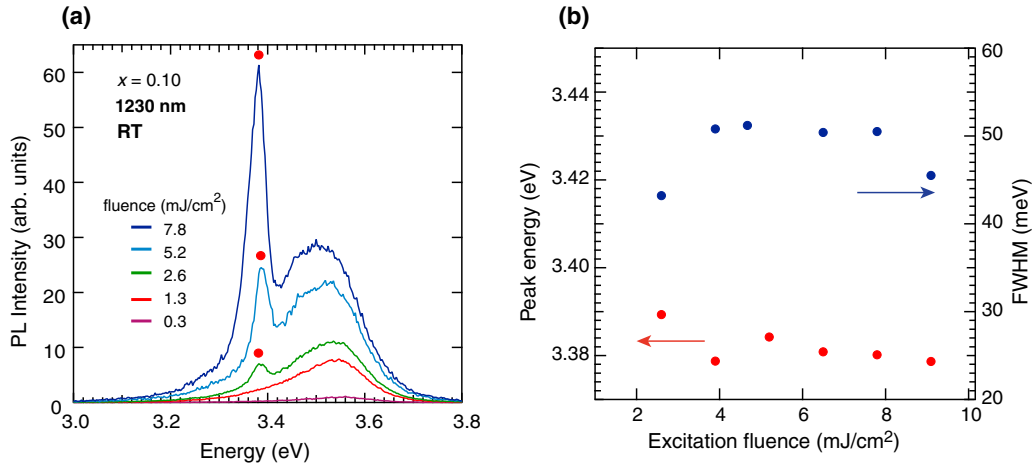


FIG. 4. (a) Changes in the room-temperature PL spectra of the  $x = 0.10$  film with  $I_{\text{exc}}$ . (b) Excitation fluence dependence of the emission peak energy (left axis) and the FWHM (right axis) of the narrow peak emerged under the excitation above  $I_{\text{exc}} > 2.6 \text{ mJ/cm}^2$ . The fourth harmonic ( $\lambda = 266 \text{ nm}$ ) of a 10-ns pulsed Nd:YAG laser was used as an excitation source.

however, that the excitation fluence dependence of the observed spectra is different depending on the film thickness. One also sees from Fig. 3(a) that the 120-nm-thick sample shows a substantial spectral broadening and redshift with increasing  $I_{\text{exc}}$ , as often observed for EHP lasing in ZnO nanostructured materials [12,14,35]. Note, however that the degree of the spectral broadening and redshift is diminished with increasing  $d$ . As shown in Figs. 3(e) and 3(f), the FWHM and the emission peak energy of the 1018-nm film are almost constant with increasing  $I_{\text{exc}}$ , at least up to  $\sim 10 \text{ mJ/cm}^2$ . This result suggests that in the  $x = 0.04$  film samples, the mechanism of the stimulated emission changes from an EHP process to an excitonic process as the film thickness is increased to the order of micrometer. A similar trend has also been found for pure ZnO [24,25], which can be attributed to the long carrier diffusion length and the low optical loss nature of the  $\mu\text{m}$ -sized ZnO crystals [24].

Figure 4(a) shows the room-temperature PL spectra of the 1230-nm-thick  $\text{Mg}_x\text{Zn}_{1-x}\text{O}$  film with the composition of  $x = 0.10$ . As the excitation fluence exceeds  $\sim 3 \text{ mJ/cm}^2$ , a narrow peak emerges on the lower energy side of the broad spontaneous emission band and shows an abrupt increase in intensity, as in the case of the  $x = 0.04$  sample. One also notices that the peak energy and the FWHM of the narrow peak are almost unchanged with increasing  $I_{\text{exc}}$  up to  $\sim 10 \text{ mJ/cm}^2$ , as demonstrated in Fig. 4(b).

Thus, we have shown that the emission bands of these  $\mu\text{m}$ -thick  $\text{Mg}_x\text{Zn}_{1-x}\text{O}$  films samples are neither severely redshifted nor broadened with increasing  $I_{\text{exc}}$ . This implies that some excitonic processes are responsible for the stimulated emission observed at room temperature. In the subsequent subsections, we will explore the low-temperature emission characteristics of these  $\mu\text{m}$ -thick  $\text{Mg}_x\text{Zn}_{1-x}\text{O}$  films samples to get a further insight into the expected excitonic stimulated emission process.

#### D. Low-temperature (3 K) emission characteristics

Figure 5 shows the PL characteristics of the  $\mu\text{m}$ -thick ( $d = 1018 \text{ nm}$ )  $\text{Mg}_x\text{Zn}_{1-x}\text{O}$  film with the composition of

$x = 0.04$  measured at a temperature of 3 K. Under low excitation fluence ( $\sim < 0.1 \text{ mJ/cm}^2$ ), several spontaneous emission bands were observed, as shown in the lower panel of Fig. 5(a). The most pronounced emission at 3.415 eV is attributed to a neutral donor bound exciton ( $D^0X$ ) [26,36], which is accompanied by a higher energy shoulder at 3.436 eV. Considering that the binding energy of the neutral donor bound exciton in ZnO and  $\text{Mg}_x\text{Zn}_{1-x}\text{O}$  is  $\sim 20 \text{ meV}$  [36], we can assign that the higher energy shoulder at 3.436 eV is due to the FX recombination. This assignment is consistent with the observation of the  $A$  ( $B$ ) free exciton absorption at  $\sim 3.44 \text{ eV}$  at 5 K, as shown in Fig. 2(a). Furthermore, the present assignment is supported by the appearance of LO phonon replicas of the FX recombination. In the lower panel of Fig. 5(a), these phonon replicas are designated as FX-LO ( $\sim 3.36 \text{ eV}$ ), FX-2LO ( $\sim 3.29 \text{ eV}$ ), and FX-3LO ( $\sim 3.22 \text{ eV}$ ), which are separated evenly by  $\sim 73 \text{ meV}$  corresponding to the LO phonon energy  $\hbar\omega_{\text{LO}}$  of the  $\text{Mg}_x\text{Zn}_{1-x}\text{O}$  alloy with  $x = 0.04$  [32] [see also Fig. 5(b)]. The observation of these phonon replicas could result not only from the high optical quality of the present  $\mu\text{m}$ -thick film but also from a high degree of ionicity of the  $\text{Mg}_x\text{Zn}_{1-x}\text{O}$  alloys [26].

When the excitation fluence is increased more than  $\sim 2 \text{ mJ/cm}^2$ , a sharp peak appears at  $\sim 3.38 \text{ eV}$ , followed by a rapid increase in intensity, as shown in the upper panel in Fig. 5(a). The peak energy of the sharp peak shows a redshift from  $\sim 3.38$  to  $\sim 3.36 \text{ eV}$  with increasing  $I_{\text{exc}}$  up to  $\sim 25 \text{ mJ/cm}^2$  [see Fig. 5(b)]. On the other hand, the FWHM remains almost constant irrespective of  $I_{\text{exc}}$  [see Fig. 5(a)]. These observations suggest that the observed spectral redshift is not due to an EHP process but to the exciton-exciton (ex-ex) scattering process, in which one exciton recombines radiatively while the other is scattered into a higher quantum state ( $n = 2, 3, \dots \infty$ ). This yields the emission of the so-called  $P(n)$  line, whose emission energy at  $T$  is given by [8]

$$P(n, T) = E_{\text{FX}}(T) - E_b \left( 1 - \frac{1}{n^2} \right) - \frac{3}{2} k_B T, \quad (2)$$

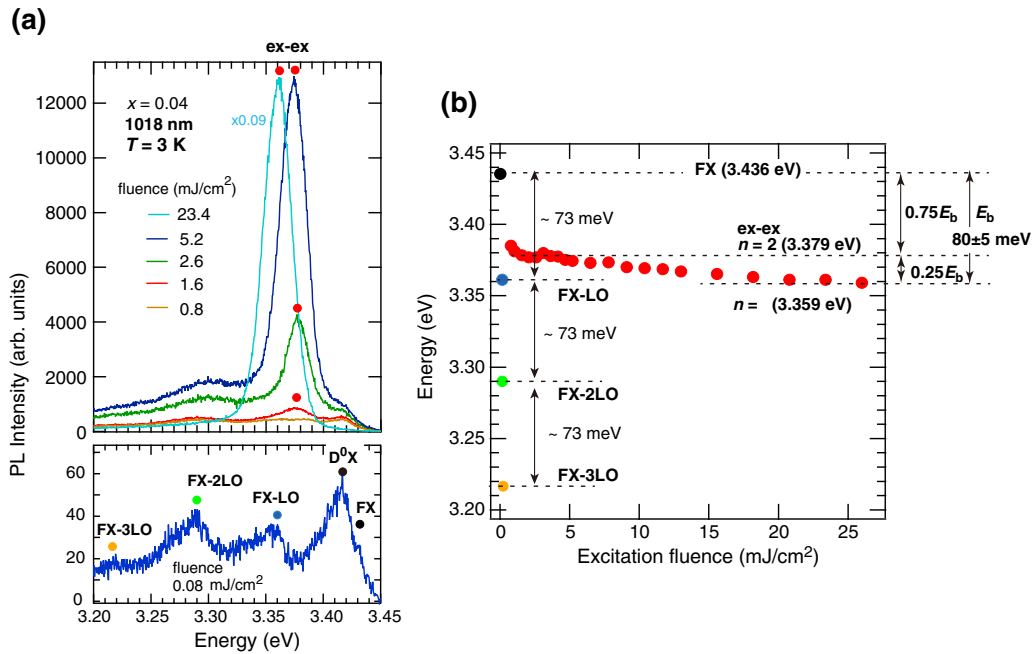


FIG. 5. PL characteristics of the  $x = 0.04$  sample ( $d = 1018$  nm) measured at 3 K. (a) Changes in the PL spectra with increasing excitation fluence from 0.08 to 23.4 mJ/cm<sup>2</sup>. (b) The peak energy of the sharp emission component marked by a red filled circle in (a) as a function of the excitation fluence. In (b), the energies of FX, FX-LO, FX-2LO, and FX-3LO shown in (a) are also indicated. The third harmonic ( $\lambda = 355$  nm) of a 10-ns pulsed Nd:YAG laser was used as an excitation source.

where  $k_B$  is the Boltzmann constant. According to Eq. (2), the energy of the emission maximum for  $n = 2$  is lower than that for  $n = \infty$  by  $E_b/4$  at constant  $T$ . Then, the observed redshift  $\Delta E$  with  $I_{\text{exc}}$  can be interpreted in terms of the transition from  $P(2)$  to  $P(\infty)$  in the ex-ex scattering process, as has been observed for the  $\mu\text{m}$ -sized ZnO particles [24,25]. Thus, the  $E_b$  value of the  $x = 0.04$  sample is estimated to be  $80 \pm 5$  meV from the value of  $\Delta E$  ( $\sim 20$  meV) [see also Fig. 5(b)]. Then, we can evaluate the FX recombination energy from  $E_b$  and  $P(\infty)$  since, according to Eq. (2),  $E_{\text{FX}} = E_b + P(\infty)$  at the low-temperature limit. The estimated value of  $E_{\text{FX}}$  is  $\sim 3.44$  eV, which is in good agreement with the observed FX absorption and recombination energies, shown in Figs. 2(a) and 5(a), respectively. Thus, our estimation of the  $E_b$  value of  $\sim 80$  meV is consistent with all the experimental data obtained for the  $x = 0.04$  sample.

We next turn to the low-temperature emission characteristics of the  $x = 0.10$  sample. It has previously been demonstrated that the spontaneous excitonic emission of  $\text{Mg}_x\text{Zn}_{1-x}\text{O}$  becomes broad with increasing  $x$  due to alloying with Mg [19,26,36], which prevents distinction between  $D^0X$  and FX emissions for the  $\text{Mg}_x\text{Zn}_{1-x}\text{O}$  samples with  $x > 0.09$ . However, it has been shown that in  $\text{Mg}_x\text{Zn}_{1-x}\text{O}$  with  $x > \sim 0.08$ , the free excitons tend to become localized in the alloy disorder potential, leading to significant longer decay times of more than  $\sim 10$  ns [37–39]. Thus, it can be possible to distinguish between  $D^0X$  and FX emissions from time-resolved PL measurements. We hence measured the time-delayed spectra of the  $x = 0.10$  sample by using the fourth harmonic ( $\lambda = 266$  nm) of a 10-ns pulsed Nd:YAG laser as an excitation source under low (0.01 mJ/cm<sup>2</sup>) excitation fluence, as shown in the upper panel in Fig. 6(a). The time-delayed PL spectra were obtained with delay times of 0 and

10 ns and a common gate width of 5 ns. When the delay time is 0 ns, one sees a broad PL band peaking at 3.59 eV, accompanied by two low-energy shoulders due probably to the LO phonon replicas of free excitons. This main peak is too broad to distinguish between  $D^0X$  and FX recombinations, as noted earlier. However, when the time-delayed PL spectrum was measured immediately after termination of the incident laser pulse, i.e., with a delay time of 10 ns, the peak energy shows a blueshift from 3.59 to 3.61 eV. The peak energy shift of 20 meV is comparable to a typical energy difference between  $D^0X$  and FX recombinations in  $\text{Mg}_x\text{Zn}_{1-x}\text{O}$  alloys [36]. The decay profile of the emission in the 3.60–3.62-eV energy region is shown in the lower panel of Fig. 6(a). We found that the blueshifted emission exhibits a single exponential decay with a time constant of  $\sim 10$  ns. Thus, we identify the high-energy peak as spontaneous recombination of (quasi)free excitons, which are localized in the alloy disorder potential and hence are characterized by longer decay times of tens of nanoseconds [38].

When  $I_{\text{exc}}$  is increased over  $\sim 2$  mJ/cm<sup>2</sup>, a new emission peak emerges at 3.52 eV [see Fig. 6(b)]. However, the emission with a decay time of  $\sim 10$  ns was missing in the 3.60–3.62-eV energy region for  $I_{\text{exc}} > \sim 2$  mJ/cm<sup>2</sup> [see the lower panel in Fig. 6(a)]. This supports our assertion that the emission process switches from spontaneous to stimulated emission with increasing excitation above threshold. We also found that upon further increase in  $I_{\text{exc}}$  to  $\sim 25$  mJ/cm<sup>2</sup>, this peak shows a redshift of  $\sim 30$  meV and its intensity relative to the  $D^0X$ /FX line substantially increases. It is probable that this energy shift is induced by the change in the scattering level from  $n = 2$  to  $n = \infty$  involved in the ex-ex process, as observed in the  $x = 0.04$  sample. From the range of redshift ( $\sim 30$  meV),  $E_b$  is estimated to be  $120 \pm 10$  meV [see

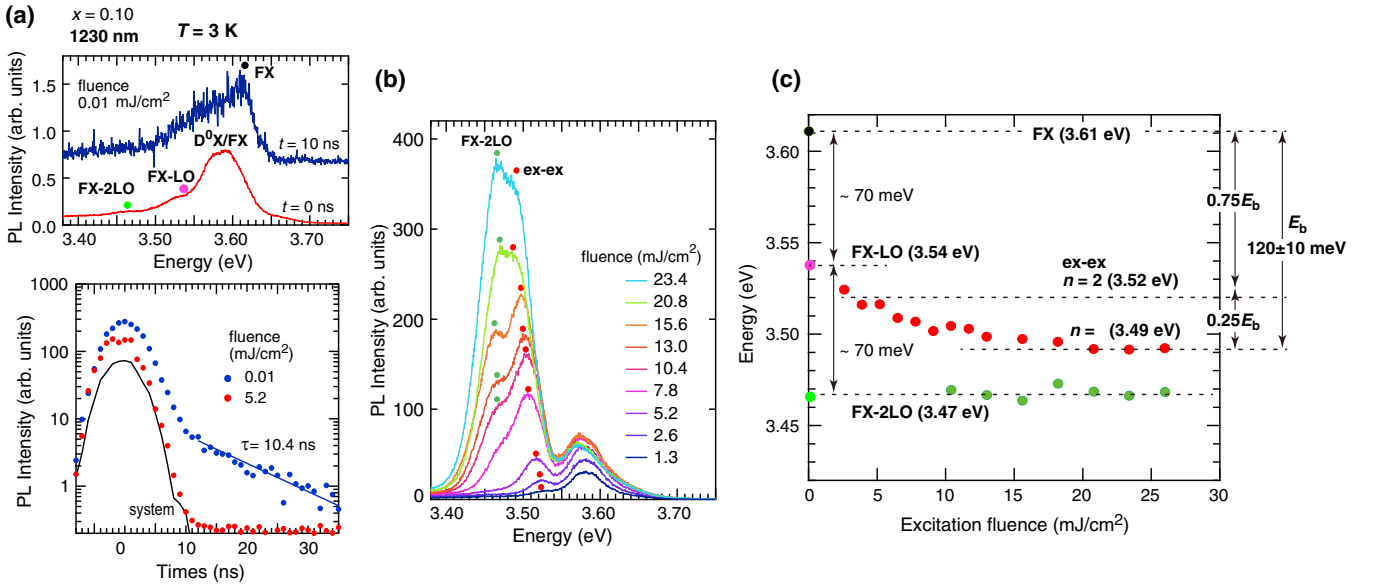


FIG. 6. 3-K PL characteristics of the  $x = 0.10$  sample ( $d = 1230$  nm) obtained under excitation with the fourth harmonic ( $\lambda = 266$  nm) of a 10-ns pulsed Nd:YAG laser. (a) Upper panel: Time-delayed PL spectra obtained with delay times of 0 ns (lower curve) and 10 ns (upper curve) and a gate width of 5 ns under excitation fluence of  $0.01$   $\text{mJ}/\text{cm}^2$ . Lower panel: The decay profile of the emission in the  $3.60$ – $3.62$ -eV energy region obtained under different excitation fluences indicated. The solid line shows an exponential fit to the tail end of the emission data, yielding the decay time constant  $\tau$  of  $10.4$  ns. (b) Changes in the PL spectra with increasing excitation fluence from  $1.3$  to  $23.4$   $\text{mJ}/\text{cm}^2$ . (c) The peak energy of the sharp emission components marked by red and dark green filled circles in (b) as a function of the excitation fluence. In (c), the energies of FX, FX-LO, and FX-2LO shown in the upper panel in (a) are also indicated.

Fig. 6(c)]. If the estimation of  $E_b$  is correct, the emission energy of the (quasi)free exciton recombination is expected to be located at  $\sim 3.61$  eV, i.e.,  $\sim 120$  meV above the  $P(\infty)$  line ( $3.49$  eV). This value is in good agreement with the recombination energy of (quasi)free excitons ( $\sim 3.61$  eV) [see the upper panel in Fig. 6(a)], giving support for the validity of the estimated value of  $E_b$ .

Figure 6(b) also demonstrates that when  $I_{\text{exc}}$  exceeds  $\sim 10$   $\text{mJ}/\text{cm}^2$  another peak develops at  $3.47$  eV, which corresponds to the energy of the FX-2LO emission line [see also Fig. 6(c)]. For  $I_{\text{exc}}$  greater than  $\sim 20$   $\text{mJ}/\text{cm}^2$ , the  $3.47$ -eV peak tends to dominate over the ex-ex line. This implies that the principal mechanism of the excitonic stimulated emission switches from the ex-ex process to the FX-2LO process with increasing  $I_{\text{exc}}$  above  $\sim 20$   $\text{mJ}/\text{cm}^2$ .

### E. Temperature dependence of the excitonic stimulated emissions

We have shown in the previous subsections the emission spectra of the  $\mu\text{m}$ -thick  $\text{Mg}_x\text{Zn}_{1-x}\text{O}$  samples at 3 and 300 K. For these samples, the ex-ex process is likely to be responsible for the observed emission at 3 K under moderate excitation conditions ( $2 \leq I_{\text{exc}} \leq 10$   $\text{mJ}/\text{cm}^2$ ). If this consideration is correct, the peak energy of the stimulated emission should obey the temperature dependence predicted by Eq. (2). In an effort to confirm this, we measured the temperature dependence of the PL spectra for both the samples in the temperature range from 3 to 300 K.

Figure 7(a) shows the temperature dependence of the intensity normalized PL spectra of the  $x = 0.04$  sample ( $d = 1018$  nm) obtained under the excitation fluence of  $10.4$   $\text{mJ}/\text{cm}^2$ .

This excitation fluence is high enough to induce stimulated emissions even at room temperature [see Fig. 3(c)]. In Fig. 7(b), the peak energies, along with the emission energies of the  $P(2)$  and  $P(\infty)$  lines predicted from Eq. (2), are plotted as a function of temperature. As mentioned in Sec. III B, the temperature dependence of  $E_{\text{FX}}$  is described by Eq. (1) using the parameters shown in Fig. 2. One sees from Fig. 7(b) that the observed peak energies almost follow the temperature dependence of the  $P(\infty)$  line in the temperature range from 3 to  $\sim 200$  K. This allows us to confirm that the ex-ex scattering process is responsible for the observed stimulated emission process in this temperature range. It should be noted, however, that the observed peak energies deviate slightly from the  $P(\infty)$  line at temperatures above  $\sim 200$  K. A similar deviation from the  $P$  line was observed in the  $\mu\text{m}$ -sized pure ZnO samples [24,25] although the deviation temperature of ZnO ( $\sim 150$  K) is lower than the present value. This phenomenon has been interpreted in terms of the temperature-induced transition from the ex-ex scattering to the ex-electron (ex-el) scattering, whose emission maximum  $\hbar\omega_{\text{max}}^{\text{ex-el}}$  is given by [8,40]

$$\begin{aligned} \hbar\omega_{\text{max}}^{\text{ex-el}}(T) &= E_{\text{FX}}(T) - \frac{1}{2} \frac{m_e + m_h}{m_e} k_B T \\ &= E_{\text{FX}}(T) - \gamma k_B T, \end{aligned} \quad (3)$$

where  $m_e$  and  $m_h$  are effective electron and hole masses, respectively, and  $\gamma$  is a constant related to the total exciton mass ( $m_e + m_h$ ) over  $m_e$ . To confirm whether the expected transition occurs in the present sample, the peak energies observed in the 200–300-K range were fitted with Eq. (3), as shown in the red solid line in Fig. 7(b). We found that

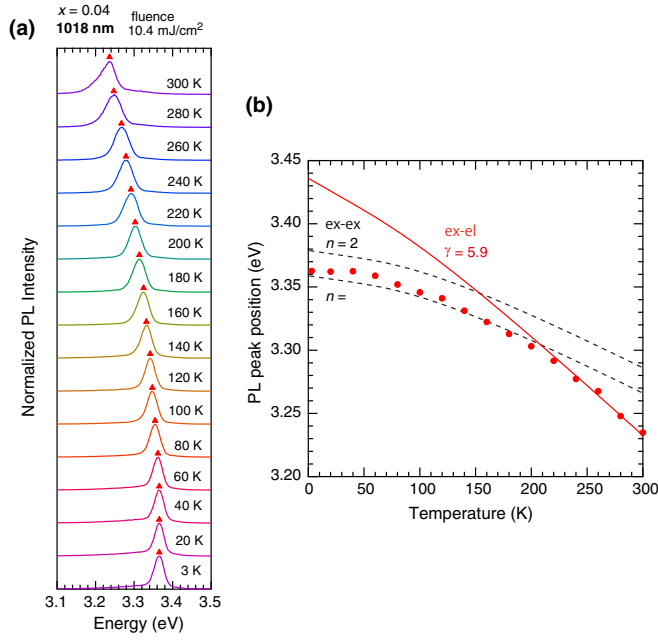


FIG. 7. (a) Changes in the PL spectra of the  $x = 0.04$  sample ( $d = 1018$  nm) with increasing temperature from 3 to 300 K measured under the excitation fluence of  $10.4$  mJ/cm<sup>2</sup>. (b) The peak energies of the PL spectra in (a) as a function of temperature. The emission energies of the ex-ex scattering process calculated from Eq. (2) are shown as broken lines. The red solid line is a fit to the data in the 200–300-K range using Eq. (3).

Eq. (3) well describes the temperature dependence of the peak energies in this temperature range. This provides support that the mechanism of the stimulated transition changes from the ex-ex process to the ex-el process with increasing temperature, similar to the case with pure ZnO [24,25]. It should be noted, however, that the transition temperature of the  $x = 0.04$  sample ( $\sim 200$  K) is much higher than that of ZnO ( $\sim 150$  K), demonstrating the higher thermal stability of the excitons in the former sample. This is in harmony with the fact that the excitons in the  $x = 0.04$  sample are characterized by a larger  $E_b$  value (80 meV) as compared with that in pure ZnO (60 meV).

Figure 8(a) illustrates the intensity-normalized PL spectra of the  $x = 0.10$  sample measured under excitation fluence of  $10.4$  mJ/cm<sup>2</sup>. Under this excitation condition, we observe two main PL bands. The higher and lower energy components represent spontaneous and stimulated emissions, respectively, as mentioned in the previous subsection. The peak energy of the lower energy component is shown in Fig. 8(b). In Fig. 8(b), the emission energies of the  $P(2)$  and  $P(\infty)$  lines predicted from Eq. (2) are also plotted as a function of temperature. As mentioned earlier, the fitted  $k$  and  $\theta$  values obtained for  $E_{\text{FX}}(T)$  of the  $x = 0.04$  sample, along with  $E_{\text{FX}}(0) = 3.61$  eV and  $E_b = 120$  meV, were used to predict the temperature dependence of  $E_{\text{FX}}$  of the  $x = 0.10$  sample.

We see from Fig. 8(b) that the peak energy of the stimulated emission almost follows the temperature dependence predicted for the  $P(\infty)$  energy in the temperature region up to  $\sim 250$  K and then shows a negative deviation from the  $P(\infty)$  line at higher temperatures. Hence, it can safely be said that

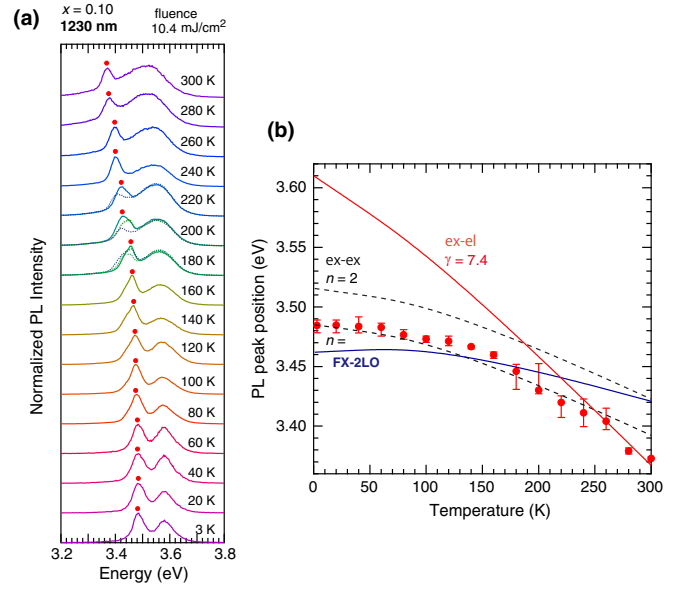


FIG. 8. Changes in the PL spectra of the  $x = 0.10$  sample ( $d = 1230$  nm) with increasing temperature from 3 to 300 K measured under excitation fluence of  $10.4$  mJ/cm<sup>2</sup>. The spectra obtained in the 180–220-K range are asymmetric and fluctuate with time, as shown, for example, as dotted line spectra. (b) The peak energies of the PL spectra in (a) as a function of temperature. The emission energies of the ex-ex scattering process calculated from Eq. (2) are shown as broken lines. The red solid line is a fit to the data in the 260–300-K range using Eq. (3). The blue solid line indicates the temperature dependence of the FX-2LO emission calculated from Eq. (4).

in the  $x = 0.10$  sample, the temperature induced transition from the ex-ex process to the ex-el process occurs at  $\sim 250$  K, which is even higher than that observed for the  $x = 0.04$  sample. This observation can be reasonably interpreted in terms of its high  $E_b$  value ( $E_b = 120 \pm 10$  meV). The temperature dependence of the stimulated emission energy in the temperature region above 260 K can be fitted with Eq. (4), as shown in Fig. 8(b), although the fitted value of  $\gamma$  may only be semiquantitatively correct because of the insufficient number of high-temperature data.

One also notices from Fig. 8(a) that the spectral shape of the stimulated emission of the  $x = 0.10$  sample tends to become asymmetric or bulging with increasing temperature from 180 K to about 220 K. In addition, the PL spectra were found to show substantial shot-to-shot fluctuations in this temperature range, as shown, for example, as the dotted line spectra in Fig. 8(a). Note, however, that at temperatures above  $\sim 250$  K, such spectral fluctuations hardly occur. These observations strongly imply that another excitonic stimulated emission process coexists with the ex-ex process in this particular temperature range, yielding asymmetric spectra that fluctuate with time. One possible candidate for the newly emerged stimulated emission process is the FX-2LO emission, as demonstrated earlier in Fig. 6(b). The expected temperature shift of the LO replicas is given by [8]

$$\hbar\omega_{\text{max}}^{\text{mLO}}(T) = E_{\text{ex}}(T) - m\hbar\omega_{\text{LO}} + \left(\frac{5}{2} - m\right)k_{\text{B}}T; \quad (4)$$

$$m = 1, 2,$$

where  $\hbar\omega_{LO}$  is the LO-phonon energy. The blue line in Fig. 8(b) shows the temperature dependence of the FX-2LO line. We assumed that the value of  $\hbar\omega_{LO}$  for the  $x = 0.10$  sample is 74 meV [32]. From Eqs. (2) and (4), it is predicted that the FX-2LO emission energy is slightly lower than the  $P(\infty)$  line by  $\sim 20$  meV at very low temperatures, e.g., 3 K. As the temperature rises, the energy difference between the FX-2LO and the  $P(\infty)$  lines is decreased and becomes close to zero at  $\sim 150$  K, as shown in Fig. 8(b). It has previously been demonstrated that the gain spectrum of the FX- $m$ LO process is highly asymmetric, extending toward low energy [41], whereas the ex-ex process gives rise to a rather symmetric gain spectrum [41]. We hence suggest that the asymmetric spectral features observed in the 180–220-K temperature range is due to the coexistence of the FX-2LO process with the ex-ex process. The gain spectra of these two processes accidentally overlap with each other in this temperature range, leading to the observed spectral asymmetry and fluctuation. When the temperature exceeds  $\sim 250$  K, the degree of overlap becomes negligible, returning to a rather symmetric spectral shape characteristics to the ex-ex process.

#### IV. DISCUSSION

From the low-temperature (3 K) PL measurements, the  $E_b$  values for the  $x = 0.04$  and  $0.10$  samples were determined to be  $80 \pm 5$  and  $120 \pm 10$  meV, respectively. This allows us to confirm that the exciton binding energy of  $\text{Mg}_x\text{Zn}_{1-x}\text{O}$  alloys increases with increasing Mg content. Previously, there have been several efforts to determine  $E_b$  of  $\text{Mg}_x\text{Zn}_{1-x}\text{O}$  alloys using, for example, temperature-dependent photoluminescence [42], optical absorption [21,43], and contactless electroreflectance techniques [19]. However, the estimated values of  $E_b$  depend strongly on the measurement techniques. Some researchers have shown that the  $E_b$  value increases with  $x$  [19,20], although the error bars are very large. Others show that  $E_b$  exhibits a negative bowing effect for increasing  $x$  [21,42] due to structural disorder [44]. The above discrepancy most likely stems from the fact that in  $\text{Mg}_x\text{Zn}_{1-x}\text{O}$ , inhomogeneous spectral line broadenings are quite large because of alloying effects [26,36]. Hence, it would be difficult, in general, to determine the exact value of  $E_b$  from the observed spectral information. In this work, the  $E_b$  values are estimated from the peak shift of the stimulated emission from the rather narrow  $P(2)$  and  $P(\infty)$  lines at 3 K. Thus, as compared to the method based on optical absorptions and spontaneous emissions, the present method will give a good estimation for  $E_b$  in  $\text{Mg}_x\text{Zn}_{1-x}\text{O}$ .

Figure 9 shows a typical relationship between  $E_b$  (in meV) and  $E_g$  (in eV) at 300 K obtained for a variety of III-V and II-VI semiconductors, demonstrating the following power-law relationship [45]

$$E_b = 4.36E_g^{1.60}. \quad (5)$$

It is hence interesting to investigate whether or not the above empirical power-law relationship can be applied to the  $E_b$  and  $E_g$  data obtained for the  $x = 0.04$  and  $0.10$  samples. We estimated  $E_g$  at 300 K for the present samples from  $E_b$ ,  $E_{FX}(0)$ , and their temperature dependence deduced from

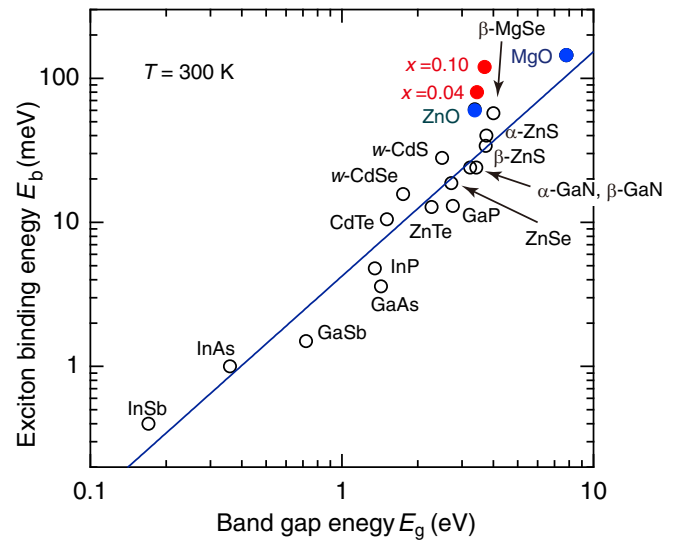


FIG. 9. Exciton binding energy  $E_b$  vs band gap energy  $E_g$  at 300 K for a variety of III-V and II-VI semiconductors (adapted from Ref. [45]). The solid line represents the power-law fit to the data, excluding those for the  $x = 0.04$  and  $0.10$  samples. The best fitted equation is  $E_b = 4.36E_g^{1.60}$  ( $E_b$  in meV;  $E_g$  in eV).

Eq. (1). The estimated  $E_g$  values for the  $x = 0.04$  and  $0.10$  samples are 3.46 and 3.68 eV, respectively. We see from Fig. 9 that the  $E_b$  and  $E_g$  data for the  $x = 0.04$  and  $0.10$  samples show a noticeable deviation from the empirical power-law relationship. In general,  $E_b$  is described as a function of  $m_e$ ,  $m_h$ , and the dielectric constant  $\epsilon$  [17]. On the other hand, according to  $\mathbf{k}\cdot\mathbf{p}$  perturbation theory,  $E_g$  is correlated linearly with the zone-center electron effective mass  $m_e^\Gamma$  [46]. Hence, it is useful to analyze how these parameters ( $m_e$ ,  $m_h$ , and  $\epsilon$ ) vary depending on  $x$ . In Fig. 7, we have shown that the fitted value of  $\gamma$ , which is proportional to  $(m_e + m_h)/m_e$  [see Eq. (3)], for the  $x = 0.04$  sample ( $\gamma = 5.9$ ) is comparable that of pure ZnO ( $\gamma \approx 6$  [18,19]). Hence, it is probable that the ratio  $m_h/m_e$  is hardly dependent on  $x$ . Considering that  $m_e$  is approximately linearly correlated with  $E_g$  [45,47], we expect that  $m_h$  also increases linearly with  $x$  (or  $E_g$ ) in view of the  $x$ -independent nature of  $m_h/m_e$ . Accordingly, the reduced mass of exciton  $\mu = (m_e m_h)/(m_e + m_h) = m_h/(1 + m_h/m_e)$  increases with  $x$ . The increase in  $\mu$  inevitably results in an increase in  $E_b$  since  $E_b$  is given by [17,47]

$$E_b = \frac{\mu}{m_0} \frac{1}{\epsilon^2} 13.6 \text{ eV}, \quad (6)$$

where  $m_0$  is the electron rest mass.

The effect of  $\epsilon$  on  $E_b$  can be more complex. In Ref. [48], it is pointed out that the static dielectric constant  $\epsilon_s$  cannot be used as  $\epsilon$  in calculating  $E_b$  when  $E_b$  is large compared to  $\hbar\omega_{LO}$ , as in the case of the present samples. In such a situation, one should use a value which interpolates between  $\epsilon_s$  and the high-frequency limit of the dielectric constant  $\epsilon_\infty$  ( $\epsilon_s \geq \epsilon \geq \epsilon_\infty$ ) depending on the distance between electron and hole [48]. It has previously been demonstrated that in  $\text{Mg}_x\text{Zn}_{1-x}\text{O}$  thin films,  $\epsilon_s$  is almost constant with  $x$  ( $\epsilon_s \approx 8$ ), whereas  $\epsilon_\infty$  shows a constant decrease with  $x$  [49]. We can hence expect that the  $\epsilon$  value that characterizes  $E_b$  in the present  $\text{Mg}_x\text{Zn}_{1-x}\text{O}$  films

will decrease with increasing  $x$ . This also leads to an increase in  $E_b$  with  $x$ .

From the discussion mentioned above, we can infer that the observed deviation of the  $E_b$  values from the empirical  $E_b - E_g$  power-law relationship results from a complex, combined effect of  $x$  on  $m_e$ ,  $m_h$ , and  $\varepsilon$ , i.e., one is a simultaneous increase in  $m_e$  and  $m_h$  with  $x$ , and the other is a decrease in  $\varepsilon$  with  $x$ .

## V. CONCLUSIONS

We have shown that purely excitonic stimulated emissions are realized in the  $\mu\text{m}$ -thick  $\text{Mg}_x\text{Zn}_{1-x}\text{O}$  ( $x = 0.04$  and  $0.10$ ) films in the temperature range from 3 to 300 K. The  $E_b$  values of the samples with compositions of  $x = 0.04$  and  $0.10$  are estimated to be  $80 \pm 5$  and  $120 \pm 10$  meV, respectively, from the low-temperature (3 K) stimulated emission characteristics due to the ex-ex scattering process. This increase in  $E_b$  leads to the higher thermal stability of the excitons in the  $\text{Mg}_x\text{Zn}_{1-x}\text{O}$

films as compared to the pure ZnO samples. Accordingly, the ex-ex process in the  $x = 0.04$  and  $0.10$  samples persists at temperatures up to  $\sim 200$  and  $\sim 250$  K, respectively. The resulting stimulated emission process is then replaced by another excitonic process or the ex-el process, thereby enabling the excitonic stimulated emission to be continued up to room temperature. Thus, in the micrometer-thick  $\text{Mg}_x\text{Zn}_{1-x}\text{O}$  films, the  $E_b$  value can be tuned from  $\sim 80$  to  $\sim 120$  meV by the appropriate control of the Mg content and the coherence length of the resulting films. A simultaneous increase in  $m_e$  and  $m_h$  along with a decrease in  $\varepsilon$  with  $x$  is most likely responsible for the realization of such large  $E_b$  values in the present micrometer-thick  $\text{Mg}_x\text{Zn}_{1-x}\text{O}$  films.

## ACKNOWLEDGMENT

We are grateful to Y. Wada, National Institute for Material Science, Japan, for his strong support in the low-temperature optical-absorption measurements.

- 
- [1] A. Teke, Ü. Özgür, S. Doğan, X. Gu, H. Morkoç, B. Nemeth, J. Nause, and H. O. Everitt, *Phys. Rev. B* **70**, 195207 (2004).
- [2] G. D. Scholes and G. Rumbles, *Nat. Mater.* **5**, 683 (2006).
- [3] A. M. Jones, H. Yu, J. R. Schaibley, J. Yan, D. G. Mandrus, T. Taniguchi, K. Watanabe, H. Dery, W. Yao, and X. Xu, *Nat. Phys.* **12**, 323 (2016).
- [4] P. Odenthal, W. Talmadge, N. Gundlach, R. Wang, C. Zhang, D. Sun, Z.-G. Yu, Z. V. Vardeny, and Y. S. Li, *Nat. Phys.* **13**, 894 (2017).
- [5] Y. Y. Kuznetsova, M. Remeika, A. A. High, A. T. Hammack, L. V. Butov, M. Hanson, and A. C. Gossard, *Opt. Lett.* **35**, 1587 (2010).
- [6] H. Morkoç and Ü. Özgür, *Zinc Oxide: Fundamentals, Materials, and Device Technology* (Wiley-VCH, Weinheim, 2009).
- [7] A. Janotti and C. G. Van de Walle, *Rep. Prog. Phys.* **72**, 126501 (2009).
- [8] C. Klingshirn, *Phys. Status Solidi B* **71**, 547 (1975).
- [9] D. M. Bagnall, Y. F. Chen, Z. Zhu, T. Yao, M. Y. Shen, and T. Goto, *Appl. Phys. Lett.* **73**, 1038 (1998).
- [10] P. Zu, Z. K. Tang, G. K. L. Wong, M. Kawasaki, A. Ohtomo, H. Koinuma, and Y. Segawa, *Solid State Commun.* **103**, 459 (1997).
- [11] D. M. Bagnall, in *Zinc Oxide Materials for Electronic and Optoelectronic Devices and Applications*, edited by C. W. Litton, D. C. Reynolds, and T. C. Collins (Wiley, Chichester, 2011), pp. 265–284.
- [12] C. Klingshirn, R. Hauschild, J. Fallert, and H. Kalt, *Phys. Rev. B* **75**, 115203 (2007).
- [13] C. Klingshirn, J. Fallert, O. Gogolin, M. Wissinger, R. Hauschild, M. Hauser, H. Kalt, and H. Zhou, *J. Lumin.* **128**, 792 (2008).
- [14] M. A. M. Versteegh, D. Vanmaekelbergh, and J. I. Dijkhuis, *Phys. Rev. Lett.* **108**, 157402 (2012).
- [15] F. Gindele, U. Woggon, W. Langbein, J. M. Hvam, K. Leonardi, D. Hommel, and H. Selke, *Phys. Rev. B* **60**, 8773 (1999).
- [16] H. D. Sun, T. Makino, N. T. Tuan, and Y. Segawa, Z. K. Tang and G. K. L. Wong, M. Kawasaki, A. Ohtomo, and K. Tamura, and H. Koinuma, *Appl. Phys. Lett.* **77**, 4250 (2000).
- [17] M. Grundmann, in *Physics of Semiconductors* (Springer, Berlin, 2006), p. 227.
- [18] M. Fox, in *Optical Properties of Solids* (Oxford University Press, New York, 2001), p. 78.
- [19] M. Wefna, R. Kudrawiec, A. Kaminska, A. Kozanecki, B. Laumer, M. Eickhoff, and J. Misiewicz, *Appl. Phys. Lett.* **103**, 251908 (2013).
- [20] M. D. Neumann, N. Esser, J.-M. Chauveau, R. Goldhahn, and M. Feneberg, *Appl. Phys. Lett.* **108**, 221105 (2016).
- [21] R. Schmidt, B. Rheinländer, M. Schubert, D. Spemann, T. Butz, J. Lenzner, E. M. Kaidashev, M. Lorenz, A. Rahm, H. C. Semmelhack, and M. Grundmann, *Appl. Phys. Lett.* **82**, 2260 (2003).
- [22] C. R. Ding, S. W. Li, and H. Z. Wang, *Appl. Phys. Lett.* **90**, 241918 (2007).
- [23] C. H. Chia, J. N. Chen, and Y. M. Hu, *Appl. Phys. Lett.* **99**, 131908 (2011).
- [24] R. Matsuzaki, H. Soma, K. Fukuoka, K. Kodama, A. Asahara, T. Suemoto, Y. Adachi, and T. Uchino, *Phys. Rev. B* **96**, 125306 (2017).
- [25] R. Matsuzaki and T. Uchino, *J. Appl. Phys.* **124**, 063103 (2018).
- [26] T. A. Wassner, B. Laumer, S. Maier, A. Laufer, B. K. Meyer, M. Stutzmann, and M. Eickhoff, *J. Appl. Phys.* **105**, 023505 (2009).
- [27] K. Yamamoto, T. Tsuboi, T. Ohashi, T. Tawara, H. Gotoh, and A. Nakamura, J. Temmyo, *J. Cryst. Growth* **312**, 1703 (2010).
- [28] Y. Xie, M. Madel, T. Zoberbier, A. Reiser, W. Jie, B. Neuschl, J. Biskupek, U. Kaiser, M. Feneberg, and K. Thonke, *Appl. Phys. Lett.* **100**, 182101 (2012).
- [29] A. Rahm, M. Lorenz, T. Nobis, G. Zimmermann, M. Grundmann, B. Fuhrmann, and F. Syrowatka, *Appl. Phys. A* **88**, 31 (2007).
- [30] W. Y. Liang and A. D. Yoffe, *Phys. Rev. Lett.* **20**, 59 (1968).
- [31] J. F. Muth, R. M. Kolbas, J. F. Muth, and R. M. Kolbas, *J. Appl. Phys.* **85**, 7884 (1999).
- [32] J. D. Ye, K. W. Teoh, X. W. Sun, G. Q. Lo, and D. L. Kwong, *Appl. Phys. Lett.* **91**, 091901 (2007).

- [33] G. D. Cody, Hydrogenated amorphous silicon, edited by J. I. Pankove, *Semiconductors and Semimetals*, Vol. 21, Part b (Academic, New York, 1984), Chap. 2, pp. 42–47.
- [34] L. Wang and N. C. Giles, *J. Appl. Phys.* **94**, 973 (2003).
- [35] T. Nakamura, K. Firdaus, and S. Adachi, *Phys. Rev. B* **86**, 205103 (2012).
- [36] M. D. Neumann, C. Cobet, N. Esser, B. Laumer, T. A. Wassner, M. Eickhoff, M. Feneberg, and R. Goldhahn, *J. Appl. Phys.* **110**, 013520 (2011).
- [37] J. Yoo, Y. J. Hong, G.-C. Yi, B. Chon, and T. Joo, *Semicond. Sci. Technol.* **23**, 095015 (2008).
- [38] A. Müller, M. Stölzel, C. Dietrich, G. Benndorf, M. Lorenz, and M. Grundmann, *J. Appl. Phys.* **107**, 013704 (2010).
- [39] A. Müller and M. Grundmann, *Phys. Rev. B* **87**, 035134 (2013).
- [40] C. I. Yu, T. Goto, and M. Ueta, *J. Phys. Soc. Jpn.* **34**, 693 (1973).
- [41] H. Haug and S. Koch, *Phys. Status Solidi b* **82**, 531 (1977).
- [42] J. G. Lu, Y. Z. Zhang, Z. Z. Ye, Y. J. Zeng, J. Y. Huang, and L. Wang, *Appl. Phys. Lett.* **91**, 193108 (2007).
- [43] C. W. Teng and J. F. Muth, Ü. Özgür, M. J. Bergmann, H. O. Everitt, A. K. Sharma, C. Jin, and J. Narayan, *Appl. Phys. Lett.* **76**, 979 (2000).
- [44] M. A. Kanehisa and R. J. Elliott, *Phys. Rev. B* **35**, 2228 (1987).
- [45] S. Adachi, in *Properties of Group-IV, III-V, and II-VI Semiconductors* (Wiley, Chichester, 2006), p. 235.
- [46] C. Hermann and C. Weisbuch, *Phys. Rev. B* **15**, 823 (1977).
- [47] J. Singh, *Semiconductor Devices: Basis Principles* (Wiley, New York, 2001), p. 54.
- [48] C. F. Klingshirm, *Semiconductor Optics*, and 2nd ed. (Springer, Berlin, 2005), pp. 241–262.
- [49] C. Bundesmann, A. Rahm, M. Lorenz, M. Grundmann, and M. Schubert, *J. Appl. Phys.* **99**, 113504 (2006).